DALTON
FULL PAPER

New intermediate-spin chloroiron(III) complex with a mixed nitrogen–sulfur co-ordination sphere ‡

Marie-Aude Kopf,[a] Daniel Varech,[a] Jean-Pierre Tuchagues,[b] Daniel Mansuy[a] and Isabelle Artaud *,†,[a]

[a] *Laboratoire de Chimie et Biochimie Pharmacologiques et Toxicologiques (URA 400 CNRS), Université René Descartes, 45 rue des Saints-Pères, 75270 Paris Cédex 06, France*
[b] *Laboratoire de Chimie de Coordination du CNRS et de l'Université Paul Sabatier, 205 route de Narbonne, 31077 Toulouse Cédex, France*

A new tetradentate proligand, 6,6′-bis(2,2-diphenyl-2-sulfanylethyl)-2,2′-bipyridine (H_2L), involving two nitrogen bases and two thiols, has been synthesized. The crystal structure of its chloroiron(III) complex [FeL(Cl)] exhibits a five-co-ordinate iron in a distorted square-pyramidal structure including a long Fe–Cl axial bond. Its effective magnetic moment ($\mu_{eff} = 3.8\ \mu_B$ from 10 to 300 K) and its Mössbauer parameters [$\delta = 0.328(5)$ mm s^{-1} and $\Delta E_Q = 2.543(9)$ mm s^{-1} at 293 K] are consistent with a pure intermediate $S = \frac{3}{2}$ spin state for the iron(III). This complex exhibits a sulfur-to-iron charge transfer absorption at 490 nm and a one-electron reduction wave at −415 mV (*vs.* SSCE). Upon reaction with tetrabutylammonium hydroxide it is converted into the μ-oxo complex [Fe_2L_2O], which has been characterized by mass spectral and elemental analyses. Its formation is reversible in dmf upon addition of trifluoroacetic acid in the presence of chloride anion, as shown by ^{1}H NMR and UV/VIS spectroscopy and electrochemistry. The [FeL(Cl)] complex appears to be the first example of an iron(III) complex with a mixed nitrogen–sulfur co-ordination sphere in a pure $S = \frac{3}{2}$ ground spin state.

With the exception of some monomeric iron-(II)[1,2] or -(III)[3,4] complexes derived from thiosalicylideneimine, the non-heme iron thiolate complexes known before 1993 were essentially iron–sulfur clusters involving iron in mixed-valence states.[5] The synthesis of mononuclear iron(III) complexes with thiolate ligands has been hampered by the easy Fe^{III}-dependent oxidation of thiolates to disulfides and the propensity of metal thiolates to give sulfur-bridged compounds.[6] Since 1993 several non-heme iron(III) complexes with a mixed nitrogen–sulfur co-ordination sphere have been reported.[7–10] One of the main objectives of their synthesis was to build chemical models of the newly characterized iron-containing nitrile hydratases. These enzymes which catalyse the hydration of nitriles to amides are the first non-heme iron enzymes with a low-spin iron(III) active site. On the basis of EPR,[11] resonance Raman,[12,13] EXAFS[12,14] and ENDOR[15,16] studies, their iron was first assumed to be six-co-ordinated with a N_3S_2O donor set, but a recent crystal structure[17] reveals that the iron center is co-ordinated to two nitrogens and three cysteines. The iron(III) complexes reported so far with a mixed nitrogen–sulfur co-ordination sphere such as N_2S_3,[10] N_3S_3,[9] or N_4S_2[8] are characterized either by a low-[8,9] or a high-spin[9,10] iron(III) state.

Herein we describe the synthesis of a new N_2S_2 tetradentate compound and the complete characterization of its chloroiron(III) complex, which appears to have a mixed nitrogen–sulfur co-ordination sphere in a pure $S = \frac{3}{2}$ ground spin state.

Experimental

Spectroscopic measurements

The UV/VIS spectra were recorded at room temperature on an Uvikon 820 spectrophotometer. Cyclic voltammograms were obtained with an EGG-PAR model 173 potentiostat and model 276 interface instruments at room temperature under argon. The electrode system consisted of a NaCl-saturated calomel electrode (SSCE) as reference, a platinum electrode as auxiliary, and a glassy carbon electrode as working electrode. The salt NBu_4BF_4 was used as supporting electrolyte (0.1 M in the appropriate solvent). The potential sweep rate was 50 mV s^{-1}. Ferrocene was used as an internal standard (under our experimental conditions, the ferrocenium–ferrocene couple is at $E_{\frac{1}{2}} =$ 450 mV *vs.* SSCE). The ^{1}H NMR spectra were recorded at 300 K on a Bruker ARX-250 spectrometer driven by UXNMR software (Bruker) on an Aspect Station 1. Chemical shifts are reported in ppm downfield from $SiMe_4$. The T_1 relaxation time measurements used an inversion–recovery pulse sequence with a relaxation delay of 0.5 s and averaging at 512 scans into a 32 K data block. The experiment was repeated for 15 values ranging from 10 ms to 1 s. The T_1 values were calculated using DISNMR software (Bruker). The calibrated value of the 360° pulse was 26 ms. X-Band EPR spectra were recorded on a Bruker ESP300 spectrometer operating at a 9.5 GHz microwave frequency, at 4 K, with a 100 kHz modulation frequency and a 1 G (10^{-4} T) modulation amplitude. The microwave power was 20 mW. Variable-temperature magnetic susceptibility data were obtained on powder polycrystalline samples with a Quantum Design MPMS SQUID susceptometer. Diamagnetic corrections were applied by using Pascal's constants. Mössbauer measurements were made on a conventional constant-acceleration spectrometer with a 25 mCi source of ^{57}Co (rhodium matrix). Isomer shift values (δ) throughout the paper are given with respect to metallic iron at room temperature. The absorber was a sample of microcrystalline powder (100 mg) enclosed in a cylindrical plastic sample holder (2 cm diameter), the size of which had been determined to optimize the absorption. Variable-temperature spectra were obtained in the 300–4.2 K range, by using a MD 306 Oxford cryostat, thermal scanning being monitored by an Oxford ITC4 servo-control device (±0.1 K accuracy). A least-squares computer program[18] was used to fit the Mössbauer parameters and determine their standard deviations of statistical origin (given in parentheses). Chemical ionization mass spectra were recorded at the Ecole Normale Supérieure in Paris and fast

† E-Mail: artaud@bisance.citi2.fr
‡ *Non-SI units employed:* Ci = 3.7×10^{10} Bq, $\mu_B \approx 9.27 \times 10^{-24}$ J T^{-1}, Oe = 10^3 A m^{-1}.

atom bombardment at the Laboratoire de spectrométrie de Masse Bioinorganique in Strasbourg, France. Elemental analyses were carried out by the microanalysis service at Paris VI University and at the Institut de Chimie des Substances Naturelles (Gif-sur-Yvette, France). The crystal structure was solved by the X-ray service of Paris VI University.

Crystallography

A selected crystal of [FeL(Cl)] **1** [H_2L = 6,6′-bis(2,2-diphenyl-2-sulfanyl ethyl)-2,2′-bipyridine] was set up on a four-circle Enraf-Nonius CAD4 diffractometer. Graphite-monochromatized Mo-Kα radiation (λ 0.710 69 Å) was used. Unit-cell dimensions with estimated standard deviations were obtained from least-squares refinements of the setting angles of 25 well centered reflections. Two standard reflections were monitored periodically and showed no change during data collection. Crystallographic data and other information is summarized in Table 1. Corrections were made for Lorentz-polarization effects. Computations were performed by using the personal computer version of CRYSTALS.[19] Atomic form factors for neutral Fe, S, Cl, N, C and H were taken from ref. 20. Real and imaginary parts of anomalous dispersion were taken into account. The structure was solved by direct methods (SHELXS)[21] and successive Fourier maps. Only some hydrogens could be found on difference maps, so they were all geometrically located and given an overall isotropic thermal parameter. Owing to the small number of reflections, only Fe, S and Cl atoms were anisotropically refined. Full-matrix least-square refinements were carried out by minimizing the function $\Sigma w(|F_o| - |F_c|)^2$ where F_o and F_c are the observed and calculated structure factors. Models reached convergence with $R = \Sigma(||F_o| - |F_c||)/\Sigma|F_o|$ and $R' = [\Sigma w(|F_o| - |F_c|)^2/\Sigma w(F_o)^2]^{\frac{1}{2}} = 0.060$ and 0.070. Criteria for a satisfactory complete analysis were the ratio of the root-mean-square shift to standard deviation being less than 0.2 and no significant feature in the last difference map.

CCDC reference number 186/870.

Synthesis

Diphenylmethanethiol **I** was synthesized according to the procedure described by Klenk *et al.*[22] Thiol **I** was protected according to the procedure described by Berg and Holm,[23] giving **III**. 6,6′Bis-(bromomethyl)-2,2′-bipyridine **II** was synthesized according to a previously described procedure.[24–26]

6,6′-Bis[2,2-diphenyl-2-(tetrahydropyran-2-ylsulfanyl)ethyl]-2,2′-bipyridine V. A solution of compound **III** (650 mg, 2.3 mmol) in anhydrous diethyl ether (10 cm^3) was cooled to −78 °C and 2.5 M $LiBu^n$ in hexane (0.9 cm^3) added dropwise. The reaction mixture was allowed to warm to 0 °C over 1 h and then cooled again to −78 °C. A solution of 6,6′-bis(bromomethyl)-2,2′-bipyridine (342 mg, 1 mmol) in thf (20 cm^3) and $P(NMe_2)_3O$ (2 cm^3), was added dropwise yielding a lightening of the reaction mixture from brown to yellow. The mixture was allowed to warm to 0 °C over 4 h and then added to water. The organic layer was set apart and the aqueous layer extracted with ethyl acetate (3 × 20 cm^3). The combined organic layers were dried over Na_2SO_4, and the solvent removed to give a yellowish oil which crystallized after addition of acetone. The product was filtered off and washed with methanol to afford 612 mg (80%) of a 1:1 mixture of diastereoisomers **A** and **B**. Recrystallization of the product from a CH_2Cl_2–MeOH mixture afforded 540 mg of a 3:2 mixture of **A** and **B**. Any further recrystallization enriched the mixture in diastereoisomer **A**. M.p. 198–200 °C (**A**:**B** = 3:2) (Found: C, 77.09; H, 6.31; N, 3.58. Calc. for $C_{48}H_{48}N_2O_2S_2$: C, 76.98; H, 6.46; N, 3.74%). Mass spectrum (CI + NH_3): *m/z* 749 (M^+, 72), 663 (5, $M - C_5H_9O - 1$) and 180 [100%, $M - 2(C_6H_5)_2CSC_5H_9O - 2$]. The ^1H NMR spectrum ($CDCl_3$) indicated the presence of two diastereoisomers: δ 7.62–7.55 (4 H, m, H^4, $H^{4'}$, H^5, $H^{5'}$), 7.26–7.11 (20 H, m, Ph), 6.75 and 6.73 (2 H, d, J = 7.5 Hz, H^3, $H^{3'}$), 4.32 and 4.26 (2 H, br s, H^{22}, $H^{22'}$), 4.18–3.87 (6 H, m, CH_2^7, $CH_2^{7'}$, H^{24} and $H^{24'}$), 3.23 (2 H, m, H^{24}, $H^{24'}$) and 1.9–1.2 (12 H, m, CH_2^{25}, CH_2^{26}, CH_2^{27}, $CH_2^{25'}$, $CH_2^{26'}$, $CH_2^{27'}$). The signals at δ 6.73 and 4.32 refer to diastereoisomer **A** and those at 6.75 and 4.26 to **B**.

6,6′-Bis(2,2-diphenyl-2-sulfanylethyl)-2,2′-bipyridine (H_2L). To a suspension of compound **V** (3 g) in ethyl acetate (80 cm^3) and methanol (60 cm^3) was added a solution of $AgNO_3$ (1.5 g, 2.5 equivalents) in pyridine (1 cm^3) and methanol (100 cm^3). The solid material dissolved immediately and the solution became yellow. After 5 h at room temperature the solvent was removed under vacuum yielding a yellow powder. The material was dissolved in deaerated dichloromethane (50 cm^3) and H_2S bubbled through the solution. The black precipitate was filtered off and washed with dichloromethane. The combined filtrates were washed with water and the aqueous layer extracted with ether. The combined organic layers were dried over $MgSO_4$ and the solvent was removed to yield 1.91 g (92%) of the product as a white powder, m.p. 202 °C (Found: C, 78.47; H, 5.6; N, 4.7. Calc. for $C_{38}H_{32}N_2S_2$: C, 78.6; H, 5.56; N, 4.82%). Mass spectrum (CI + NH_3): *m/z* 581 (M^+, 56), 547 (12, $M - SH - 1$), 383 [17, $M - (C_6H_5)_2CSH + 1$], 199 (100, $M - CH_2bipyCH_2$) and 183 [10%, $M - 2(C_6H_5)_2CSH + 1$]. ^1H NMR, [$(CD_3)_2SO$]: δ 7.72 (2 H, d, J = 7.5, H^5, $H^{5'}$), 7.55 (2 H, t, J = 7.5 Hz, H^4, $H^{4'}$), 7.45–7.3 (8 H, m, *o*-H of Ph), 7.3–7.15 (12 H, m, *m*- and *p*-H of Ph), 6.79 (2 H, d, H^3 and $H^{3'}$), 4.1 (2 H, br s, 2 SH) and 4.05 (4 H, s, CH_2^7, $CH_2^{7'}$). The resonance at δ 4.1 disappeared upon addition of D_2O.

[6,6′-Bis(2,2-diphenyl-2-sulfanylethyl)-2,2′-bipyridinato]-chloroiron(III) 1. A solution of H_2L (100 mg, 0.172 mmol, 1 equivalent), freshly prepared by deprotection of compound **V**, in anhydrous dmf (10 cm^3), was added under argon to a suspension of sodium hydride (8.2 mg, 2 equivalents) in anhydrous dmf (10 cm^3). The solid material dissolved within 15 min at room temperature. A solution of $FeCl_3$ (27.9 mg, 1 equivalent) in anhydrous dmf (5 cm^3) was then added under argon. A deep red solution was obtained. The mixture was stirred for 1 h at room temperature under argon and then exposed to the air. The volume was then reduced to about 10 cm^3. Addition of this solution to ether (100 cm^3) led to the precipitation of a brown powder, which was filtered off and washed with ether. The powder complex was dissolved in anhydrous CH_2Cl_2, in which the NaCl salt formed during the metal insertion was insoluble and thus removed by filtration. The solvent was then slowly evaporated to yield 70 mg (60%) of complex **1** as black microcrystals (Found: C, 67.98; H, 4.59; Cl, 5.53; N, 4.05; S, 9.53. Calc. for $C_{38}H_{30}ClFeN_2S_2$: C, 68.11; H, 4.51; N, 4.18; Cl, 5.29; S, 9.57%). Mass spectrum (FAB^+): *m/z* 634, (76, $FeN_2S_2Cl - Cl$), 601 (67, $FeN_2S_2Cl - Cl - HS$) and 570 (100%, $FeN_2S_2Cl - Cl - 2S$).

μ-Oxo-bis{[6,6′-bis(2,2-diphenyl-2-sulfanylethyl)-2,2′-bipyridinato]iron(III)} 2. To a solution of complex **1** (25 mg) in anhydrous CH_2Cl_2 (10 cm^3) was added under argon 1 M tetrabutylammonium hydroxide (37.3 μl) in methanol. Complex **2** precipitated as a brown powder, which was filtered off and washed with water, yield 70% (Found: C, 68.41; H, 5.03; N, 4.01; S, 9.33. Calc. for $C_{76}H_{60}Fe_2N_4OS_4 \cdot 2H_2O$: C, 69.09; H, 4.85; N, 4.24; S, 9.67%). Mass spectrum (FAB^+): *m/z* 1269 (20, $Fe_2N_4S_4O - O + 1$), 1236 (6, $Fe_2N_4S_4O - O - S$), 634 (30, FeN_2S_2), 601 (100, $FeN_2S_2 - HS$) and 568 (60%, $FeN_2S_2 - 2HS$).

Reversibility of complex 2 formation

The addition of NBu_4OH in dmf at room temperature directly, in the electrochemical cell, UV cuvette or NMR tube, to complex **1** at the concentration required for each spectroscopic technique was carried out. Then trifluoroacetic acid (tfa) was

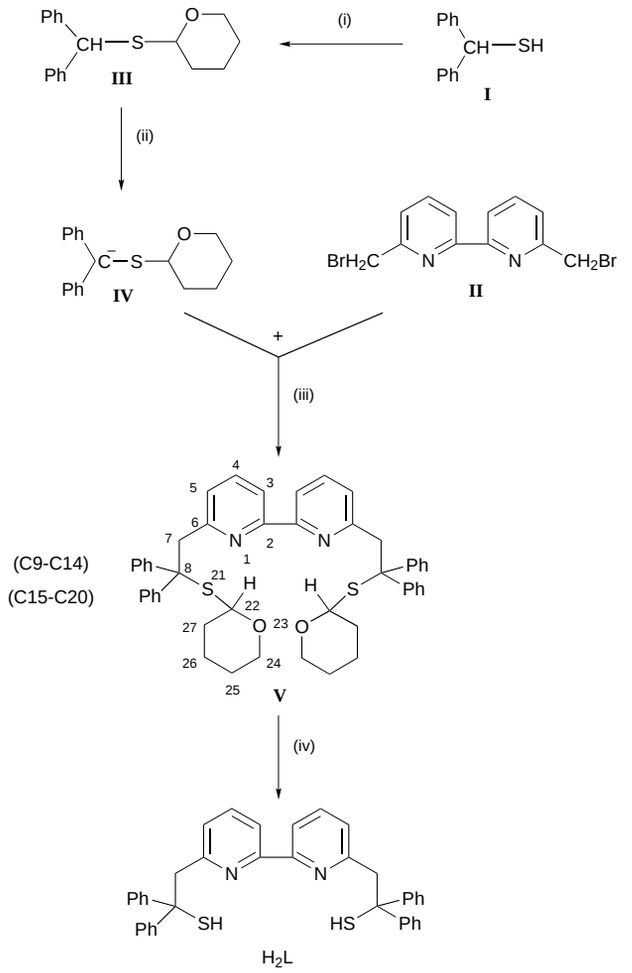

Scheme 1 Synthesis of the proligand H_2L: (i) 2,3-dihydropyran, pyridinium toluene-*p*-sulfonate, CH_2Cl_2; (ii) $LiBu^n$, ether; (iii) thf, $P(NMe_2)_3O$; (iv) $AgNO_3$, MeOH–ethyl acetate, H_2S, CH_2Cl_2

directly added without isolating complex **2**, as follows: UV/VIS, 6.5×10^{-2} mM **1** in dmf (3 cm^3) − 0.1 M NBu_4OH (2 μl) in methanol–toluene, 0.1 M tfa (2 μl) in dmf; electrochemistry, 1 mM **1** in dmf (3 cm^3) − 1 M NBu_4OH (3 μl) in methanol, 0.1 M tfa (30 μl) in dmf; NMR, 5 mM **1** in [$^2H_7$]dmf (0.5 cm^3) − 1 M NBu_4OH (2.5 μl) in methanol, 0.1 M tfa (25 μl) in dmf.

Results

Synthesis of the tetradentate proligand H_2L

The design of the proligand H_2L was derived from that reported for a tridentate NS_2H_2 compound previously synthesized by Berg and Holm[23] to model the active site and the chemical reactivity of molybdenum oxotransferases. The synthesis of the latter 2,6-bis(2,2-diphenyl-2-sulfanylethyl)pyridine was based on the reaction of 2,6-bis(bromomethyl)pyridine with the protected form **III** of diphenylmethanethiol **I**. Our proligand has been prepared by reaction of the protected thiol **III** with 6,6′-bis(bromomethyl)-2,2′-bipyridine **II** as depicted in Scheme 1. Reaction of the carbanion **IV** resulting from the lithiation of **III** at the *gem*-diphenylcarbon atom with **II**, afforded the doubly protected dithiol **V** in 80% yield from **II**. Deprotection of **V** gave the proligand H_2L in 92% yield. This compound is unstable upon standing in air and has to be stored in its protected form **IV**. This new tetradentate proligand has been completely characterized by ^1H NMR spectroscopy, mass spectrometry and elemental analysis (see Experimental section).

Synthesis of complex 1, [FeL(Cl)]

Synthesis of the corresponding iron complex has been carried out under argon. Addition of 1 equivalent of iron(III) chloride to the L^{2-} ligand in dmf yielded a deep purple solution. The complex was first precipitated from dmf by anhydrous ether, purified by dissolution in CH_2Cl_2 to eliminate sodium chloride formed during iron insertion, and finally isolated after evaporation of the solvent under vacuum. Complex **1** (60% yield) was characterized by elemental analysis and mass spectrometry. It is air stable in the solid state and in CH_2Cl_2 or dmf solution.

Table 1 Crystallographic data for complex **1**

Formula	$C_{38}H_{30}ClFeN_2S_2$
M	670.09
Crystal system	Monoclinic
Space group	$P2_1/c$
a/Å	14.695(3)
b/Å	15.135(5)
c/Å	16.141(6)
β/°	116.24(3)
U/Å^3	3220(4)
Z	4
Crystal shape	Parallelepiped
Crystal colour	Dark blue
μ/cm^{-1}	7.04
D_c/g cm^{-3}	1.38
Scan type	ω–2θ
Scan range/°	0.8 + 0.345 tan θ
θ Limits/°	1–25
T/°C	Room temperature
Octants collected	h −17 to 15, k 0–17, l 0–19
No. data collected	6120
No. unique data	5653
No. unique data used for refinement	1684 [$(F_o)^2 > 3\sigma(F_o)^2$]
R_{int}	0.052
Decay of standard reflections	None
R	0.060
R' *	0.070
Extinction parameter	119
Goodness of fit	1.14
No. variables	199
$\Delta\rho_{min}$, $\Delta\rho_{max}$/e Å^3	−0.35, 0.34

* Weighting scheme of the form $w = w'[1 - (||F_o| - |F_c||)/6\sigma(F_o)^2]^2$ with $w' = 1/\Sigma_r\Lambda_r T_r(X)$ with coefficients 3.85, −0.902 and 2.74 for a Chebyshev series for which $X = F_o/F_{o(max)}$.

Structure of complex 1

Single crystals of complex **1**, suitable for X-ray crystallography, were obtained by slow evaporation of a CH_2Cl_2 solution under a stream of argon. The complex crystallizes in the monoclinic space group $P2_1/c$. Fig. 1 shows its structure. The iron is in a distorted square-pyramidal environment with the two nitrogen atoms and the two sulfur atoms of the ligand close to the mean equatorial plane, and the chlorine atom in the axial position. The iron atom is approximately 0.48 Å out of the mean equatorial N_2S_2 plane toward the axial Cl. The two Fe–S bonds are equivalent with an average length of 2.221 Å while the two Fe–N bonds are inequivalent with lengths of 2.076(8) and 2.027(8) Å. Finally the Fe–Cl distance [2.306(3) Å] is very long compared to other ones. Selected interatomic bond lengths and angles are listed in Table 2.

Electrochemistry of complex 1

The cyclic voltammogram of complex **1** in dmf in the presence of ferrocene as internal standard exhibits two waves, with a peak to peak separation of 100 mV, which can be described as two one-electron quasi-reversible reduction steps (Fig. 2). The first one at $E_{\frac{1}{2}}$ −415 mV ($E_{\frac{1}{2}}$ *vs.* SSCE) is attributed to the Fe^{III}–Fe^{II} reduction and the second one at $E_{\frac{1}{2}}$ −1445 mV (*vs.* SSCE) to the Fe^{II}–Fe^{I} redox couple.

Table 2 Selected bond distances (Å) and angles (°) in complex **1**

Fe–S(1)	2.226(3)	Fe–Cl	2.306(3)	Fe–N(1)	2.027(8)		
Fe–S(1′)	2.217(3)			Fe–N(1′)	2.076(8)		
S(1)–C(8)	1.86(1)	S(1′)–C(8′)	1.83(1)	C(17)–C(18)	1.32(2)	C(18)–C(19)	1.41(2)
N(1)–C(2)	1.32(1)	N(1)–C(6)	1.35(1)	C(19)–C(20)	1.43(2)	C(2′)–C(3′)	1.37(2)
N(1′)–C(2′)	1.36(1)	N(1′)–C(6′)	1.32(1)	C(3′)–C(4′)	1.39(2)	C(4′)–C(5′)	1.40(2)
C(2)–C(3)	1.41(2)	C(2)–C(2′)	1.47(2)	C(5′)–C(6′)	1.39(1)	C(6′)–C(7′)	1.48(1)
C(3)–C(4)	1.39(2)	C(4)–C(5)	1.37(2)	C(7′)–C(8′)	1.58(1)	C(8′)–C(9′)	1.51(1)
C(5)–C(6)	1.40(2)	C(6)–C(7)	1.51(2)	C(8′)–C(15′)	1.56(1)	C(9′)–C(10′)	1.41(1)
C(7)–C(8)	1.52(2)	C(8)–C(9)	1.54(2)	C(9′)–C(14′)	1.40(2)	C(10′)–C(11′)	1.38(2)
C(8)–C(15)	1.52(2)	C(9)–C(10)	1.38(2)	C(11′)–C(12′)	1.34(2)	C(12′)–C(13′)	1.37(2)
C(9)–C(14)	1.36(2)	C(10)–C(11)	1.41(2)	C(13′)–C(14′)	1.40(2)	C(15′)–C(16′)	1.37(2)
C(11)–C(12)	1.29(2)	C(12)–C(13)	1.32(12)	C(15′)–C(20′)	1.36(2)	C(16′)–C(17′)	1.44(2)
C(13)–C(14)	1.48(2)	C(15)–C(16)	1.36(2)	C(17′)–C(18′)	1.32(2)	C(18′)–C(19′)	1.33(2)
C(15)–C(20)	1.36(2)	C(16)–C(17)	1.40(2)	C(19′)–C(20′)	1.42(2)		
S(1)–Fe–S(1′)	79.1(1)	S(1)–Fe–N(1′)	141.2(3)	S(1)–Fe–N(1)	91.7(3)	N(1)–Fe–N(1′)	80.0(3)
S(1′)–Fe–Cl	104.0(1)	Cl–Fe–N(1′)	101.9(3)	Cl–Fe–N(1)	95.3(3)		
S(1′)–Fe–N(1)	160.7(3)	S(1)–Fe–Cl	116.7(1)	S(1′)–Fe–N(1′)	96.5(2)		
Fe–S(1)–C(8)	110.5(4)	Fe–S(1′)–C(8′)	109.4(3)	C(16)–C(17)–C(18)	120.2(13)	C(17)–C(18)–C(19)	121.5(15)
Fe–N(1)–C(2)	114.6(7)	Fe–N(1)–C(6)	125.7(8)	C(18)–C(19)–C(20)	115.8(15)	C(15)–C(20)–C(19)	122.9(14)
Fe–N(1′)–C(6′)	127.2(7)	Fe–N(1′)–C(2′)	113.1(7)	N(1′)–C(2′)–C(2)	114.1(10)	N(1′)–C(2′)–C(3′)	122.7(11)
C(2)–N(1)–C(6)	119.5(9)	C(2′)–N(1′)–C(6′)	119.4(9)	C(2)–C(2′)–C(3′)	123.2(11)	C(2′)–C(3′)–C(4′)	118.8(11)
N(1)–C(2)–C(3)	123.4(11)	N(1)–C(2)–C(2′)	117.1(10)	C(3′)–C(4′)–C(5′)	118.0(12)	C(4′)–C(5′)–C(6′)	119.9(11)
C(3)–C(2)–C(2′)	119.4(11)	C(2)–C(3)–C(4)	115.6(12)	N(1′)–C(6′)–C(5′)	121.1(10)	N(1′)–C(6′)–C(7′)	119.8(10)
C(3)–C(4)–C(5)	121.9(13)	C(4)–C(5)–C(6)	118.4(13)	C(5′)–C(6′)–C(7′)	119.1(10)	C(6′)–C(7′)–C(8′)	111.5(9)
N(1)–C(6)–C(5)	121.7(11)	N(1)–C(6)–C(7)	118.1(10)	S(1′)–C(8′)–C(7′)	108.8(7)	S(1′)–C(8′)–C(9′)	114.2(7)
C(5)–C(6)–C(7)	120.7(11)	C(6)–C(7)–C(8)	111.2(10)	C(7′)–C(8′)–C(9′)	106.8(8)	S(1′)–C(8′)–C(15′)	102.8(7)
S(1)–C(8)–C(7)	109.1(8)	S(1)–C(8)–C(9)	112.4(8)	C(7′)–C(8′)–C(15′)	111.6(9)	C(9′)–C(8′)–C(15′)	112.6(9)
C(7)–C(8)–C(9)	108.7(9)	S1–C(8)–C(15)	104.9(7)	C(8′)–C(9′)–C(10′)	119.6(10)	C(8′)–C(9′)–C(14′)	122.3(10)
C(7)–C(8)–C(15)	111.7(9)	C(9)–C(8)–C(15)	110.0(9)	C(10′)–C(9′)–C(14′)	118.0(10)	C(9′)–C(10′)–C(11′)	119.8(11)
C(8)–C(9)–C(10)	116.1(12)	C(8)–C(9)–C(14)	122.7(12)	C(10′)–C(11′)–C(12′)	120.7(12)	C(11′)–C(12′)–C(13′)	122.4(14)
C(10)–C(9)–C(14)	121.1(13)	C(9)–C(10)–C(11)	117.1(16)	C(12′)–C(13′)–C(14′)	118.1(13)	C(9′)–C(14′)–C(13′)	121.0(12)
C(10)–C(11)–C(12)	121.6(20)	C(11)–C(12)–C(13)	125.3(22)	C(8′)–C(15′)–C(16′)	121.3(10)	C(8′)–C(15′)–C(20′)	118.3(10)
C(12)–C(13)–C(14)	116.3(19)	C(9)–C(14)–C(13)	118.8(14)	C(16′)–C(15′)–C(20′)	120.3(11)	C(15′)–C(16′)–C(17′)	118.3(12)
C8–C(15)–C(16)	125.6(11)	C(8)–C(15)–C(20)	117.1(11)	C(16′)–C(17′)–C(18′)	120.5(13)	C(17′)–C(18′)–C(19′)	121.1(13)
C(16)–C(15)–C(20)	117.3(12)	C(15)–C(16)–C(17)	122.2(12)	C(18′)–C(19′)–C(20′)	120.4(13)	C(15′)–C(20′)–C(19′)	119.2(12)

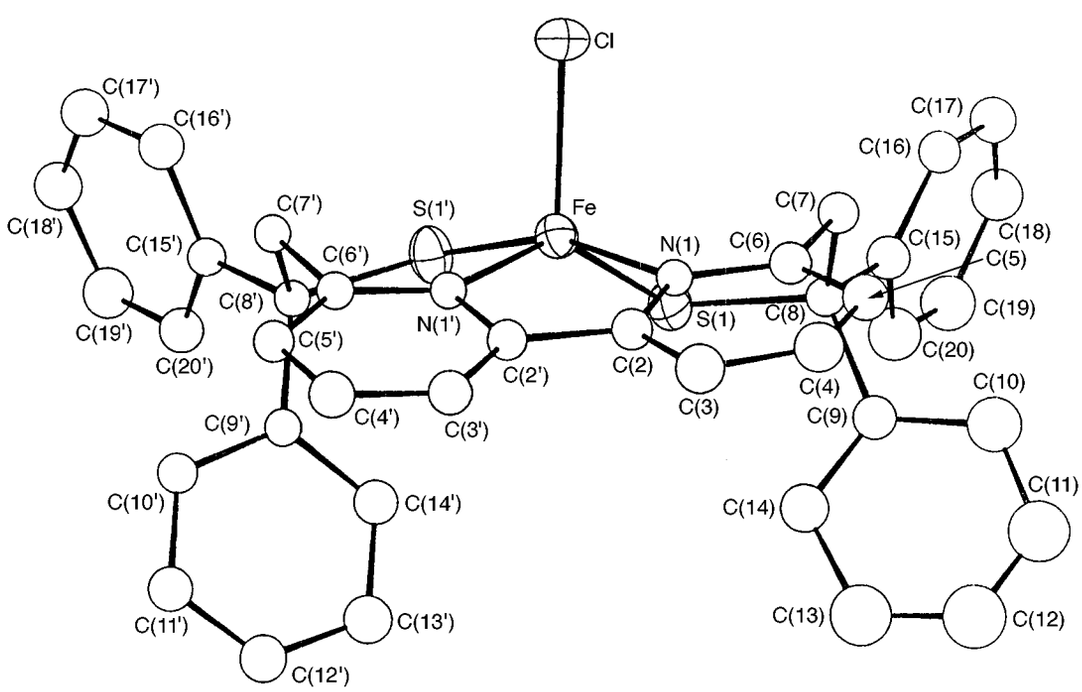

Fig. 1 Crystal structure of complex **1** with atom labeling. For clarity the hydrogen atoms are omitted

UV/VIS spectroscopy

The electronic spectrum of complex **1** is characterized by an absorption at 490 nm ($\varepsilon = 7900 \pm 350$ M^{-1} cm^{-1}) which can be assigned to a sulfur-to-iron charge-transfer band [Fig. 3(A)].

^{1}H NMR spectroscopy

The ^{1}H NMR spectrum of complex **1** in CD_2Cl_2 displays three shifted resonances of equal intensity at δ 40 (2 H), -6 (2 H) and −24 (2 H) [Fig. 4(A)]. The proton resonances of the ligand were assigned from their chemical shifts, intensity ratios and ^{1}H

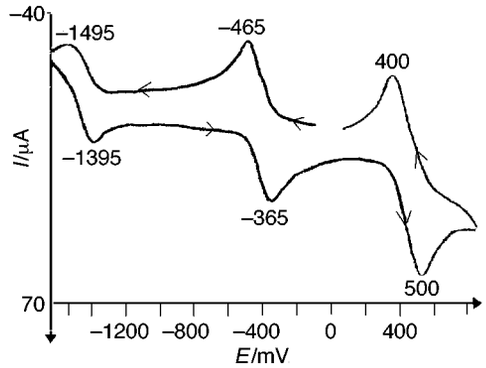

Fig. 2 Cyclic voltammogram of complex **1** (1 mM in deaerated dmf, 0.1 M NBu_4BF_4) at a glassy-carbon electrode. Potential sweep rate 50 mV s^{-1}. The ferrocenium–ferrocene couple used as internal standard is observed at +450 mV (*vs.* SSCE)

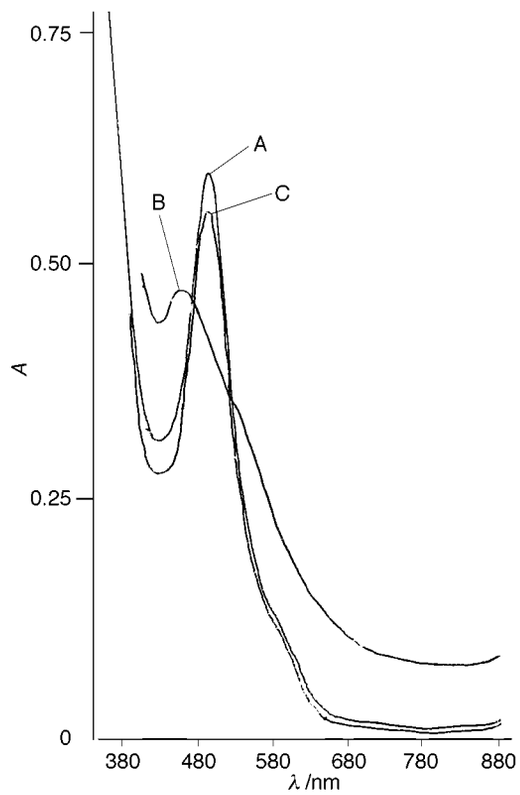

Fig. 3 Electronic spectra at 298 K in dmf of (A) 65 μM complex **1**, (B) complex **2** prepared from (A) + 1 equivalent NBu_4OH and (C) (B) + 1 equivalent tfa

longitudinal relaxation times (T_1) which have been correlated to the Fe···H distances available from the crystal structure (Table 3). In this assignment the signals with the shortest T_1 values (<7 ms) are associated with the protons closest to the iron (d < 4.3 Å). Complex **1** has almost the same symmetry as that of the proligand with a pseudo-C_2 axis. Nevertheless, the two protons bound to the C(7) [or C(7′)] carbons are inequivalent with a Fe···H distance of 4.244 Å for H(71) and 2.973 Å for H(72). The signal at δ − 6 corresponding to the shortest T_1 relaxation time (<1 ms) is attributed to the H(72) and H(7′2) protons which are closest to the iron. Similarly, the resonances at δ − 24.07 (T_1 = 6.77) and 40.45 (T_1 = 1.4 ms) are assigned to the H(71) and H(7′1) protons bound to the C(7) and C(7′) carbons, and to the protons of the phenyl rings H(14) and H(14′) {d[Fe···H(14)] = 3.599 Å}, respectively. Finally, the signals between δ 0 and 10 are attributed to the protons of the pyridine and phenyl moieties which are the farthest from the iron [d(Fe···H) > 5 Å)] and so have the largest T_1 values (22–142.7 ms).

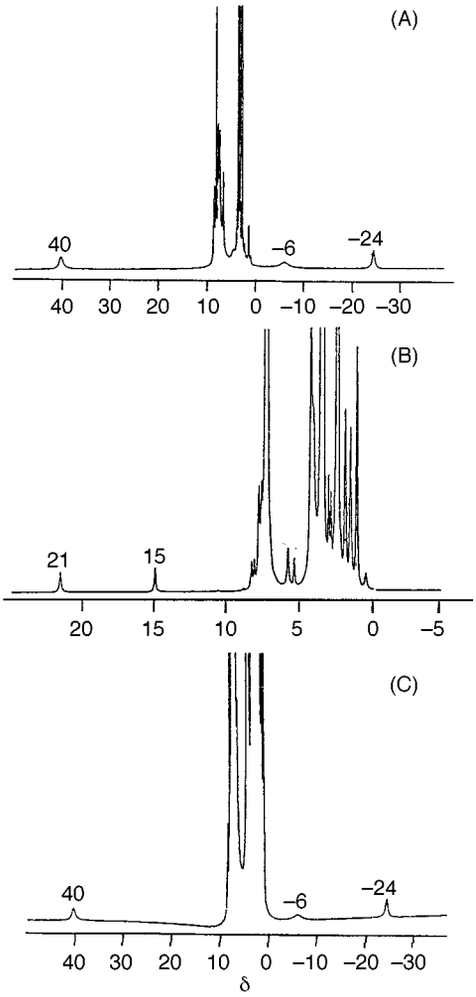

Fig. 4 Proton NMR spectra in [$^2H_7$]dmf at 300 K of (A) 5 mM complex **1**, (B) complex **2** obtained from (A) + 1 equivalent NBu_4OH and (C) (B) + 1 equivalent tfa

Magnetic susceptibility measurements

The variation of the magnetic susceptibility of complex **1** in the solid state has been measured in the 2–300 K temperature range. As shown in Fig. 5, above 10 K the effective magnetic moment reaches a constant value of 3.8 μ_B, which is, within the experimental error, the theoretical spin-only value expected for three unpaired electrons $S = \frac{3}{2}$ (3.87 μ_B). This behavior clearly shows that complex **1** is in a pure $S = \frac{3}{2}$ spin state with no spin crossover and no participation of the higher spin state. Below 10 K the moment decreases to *ca.* 3.2 μ_B at 2 K, which presumably results from a significant zero-field splitting leading to an unequal population of the Kramer's doublets of the $S = \frac{3}{2}$ spin state.

Mössbauer spectroscopy

Mössbauer spectra of complex **1** recorded at 293, 80 and 4.5 K consist of a single asymmetric quadrupole-split doublet as exemplified by the 80 K spectrum shown in Fig. 6. Although the asymmetry decreases with decreasing temperature, the broader low-energy absorption shows that the electronic system has not yet reached the fast fluctuation limit at 4.5 K.[27] The spectra were least-squares fitted with Lorentzian lines and the resulting isomer shift (δ) and quadrupole splitting parameters (ΔE_Q) are listed in Table 4 together with Mössbauer parameters gathered from the literature for square-pyramidal non-heme iron(III) complexes. The magnitudes of δ and ΔE_Q are comparable to those observed for well characterized pure $S = \frac{3}{2}$ spin systems[28] with an orbitally non-degenerate spin-quartet ground electronic state (Table 4 and refs. therein). This conclusion is further

Table 3 Proton NMR data for complex **1**

H(*xy*) [H(*x′y*)]	*d*[Fe · · · H(*xy*)] {*d*[Fe · · · H(*x′y*)]}/Å	δ (integration ratio)	T_1/ms
71	4.244	−24.07	6.77
[7′1]	{4.329}	(1 H)	
72	2.973	−6	<1
[7′2]	{3.148}	(1 H)	
14	3.599	40.45	1.4
[14′]	{3.200}	(1 H)	
Other H			
(Phenyl)	4.850–8.067	1.51–8.39 (10 H)	22–142.7
(Pyridine)	4.942–5.826		

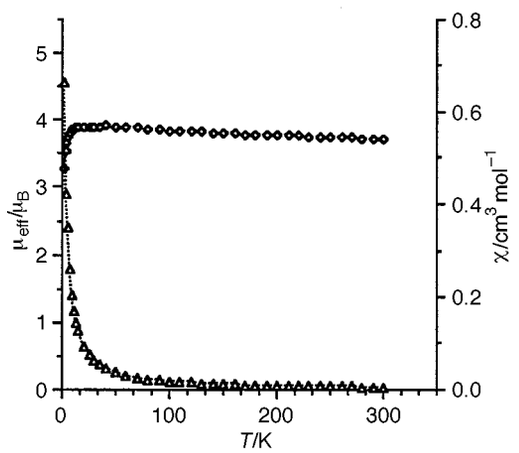

Fig. 5 Temperature dependence of the magnetic susceptibility and of the effective magnetic moment for complex **1**

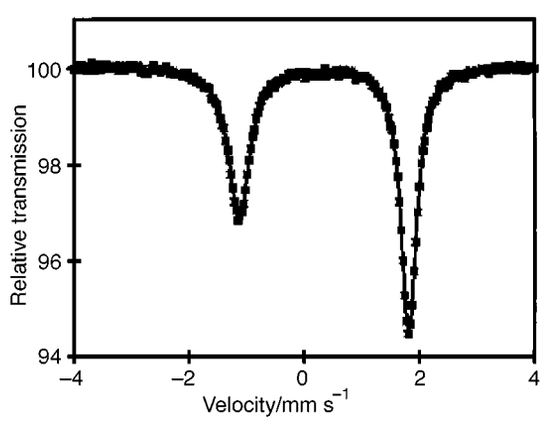

Fig. 6 Mössbauer spectrum of complex **1** recorded at 80 K in zero field

supported by the magnetic susceptibility results in the previous subsection.

EPR spectroscopy

The powder X-band EPR spectrum of complex **1** exhibits a very weak absorption at $g = 2$ and a broad and unsymmetrical signal at low field, the pattern of which is clearly temperature dependent. While two maxima are located at $g = 4.2$ and 3.4 at room temperature [Fig. 7(A)], a broad absorption centered at $g = 3.3$ with a shoulder at $g = 4.1$ is observed at 100 K (data not shown). At 4 K the EPR spectrum of the powder is nearly identical to that of the CH_2Cl_2 frozen solution which is not better resolved and exhibits a very broad resonance with a maximum at $g = 3.8$ and a weak shoulder at $g = 5.1$ [Fig. 7(B)].

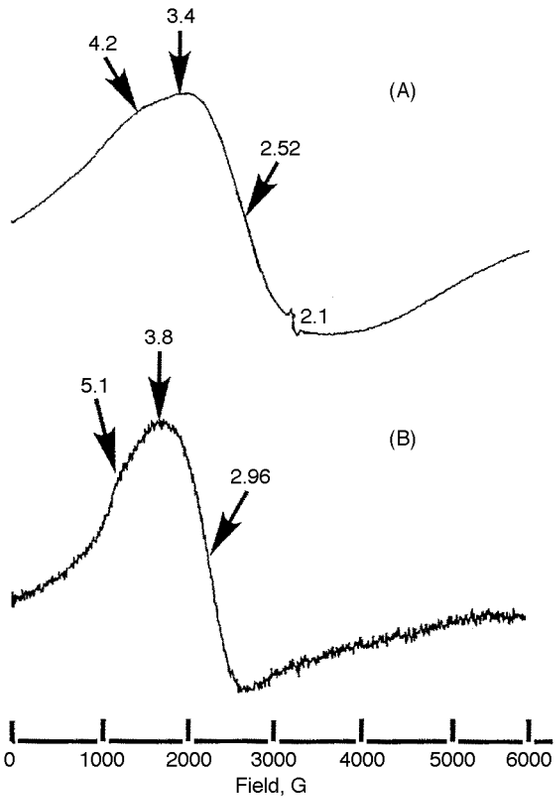

Fig. 7 X-Band EPR spectra of (A) complex **1** in the solid state at 293 K, (B) a CH_2Cl_2 frozen solution of **1** (5 mM) at 4 K

Reversible formation of the μ-oxo complex

Addition of tetrabutylammonium hydroxide to a CH_2Cl_2 solution of complex **1** leads to the precipitation of a new species **2** identified as a μ-oxo complex on the basis of its mass spectrum and elemental analyses. Complex **2** is soluble in dmf and has been further characterized in this solvent. It is EPR silent and its electronic spectrum exhibits a charge-transfer band blue-shifted from 490 to 465 nm [Fig. 3(B)]. The redox potential of the Fe^{III}–Fe^{II} couple determined by cyclic voltammetry is shifted from −415 (for complex **1**) to −740 mV (*vs.* SSCE). Such a negative redox potential has been previously reported for the complex [Fe^{III}(salen)(OH)]($E_{\frac{1}{2}} = -870$ mV *vs.* SCE), the Fe^{III}–Fe^{II} wave of which is also 520 mV cathodically shifted relative to that of the [Fe^{III}(salen)Cl] parent complex.[32] The ^{1}H NMR spectrum of complex **2** in [$^2H_7$]dmf, shown in Fig. 4(B), is characterized by two resonances at low field at δ +15 and +21.

When formed *in situ* upon addition of 1 equivalent of tetrabutylammonium hydroxide to a dmf solution of complex **1**, complex **2** reverted back to **1** after subsequent addition of 1 equivalent of trifluoroacetic acid [equation (1)]. All the

$$\underset{\mathbf{1}}{[FeL(Cl)]} \underset{CF_3CO_2H,\ dmf,\ Cl^-}{\overset{NBu_4OH,\ dmf}{\rightleftharpoons}} \underset{\mathbf{2}}{[Fe_2L_2O]} \qquad (1)$$

characteristics of complex **1** were recovered as shown by UV/VIS [Fig. 3(C)] and ^{1}H NMR [Fig. 4(C)] spectroscopy and cyclic voltammetry (data not shown).

Discussion and Conclusion

This paper describes the synthesis, structure and spectroscopic properties of a chloroiron(III) complex in a mixed nitrogen–sulfur co-ordination environment with a $S = \frac{3}{2}$ ground state. There are very few examples of such iron(III) complexes with a $S = \frac{3}{2}$ spin state. With the exception of some iron(III) porphyrins.[29,33,34] *o*-bis(dialkyldithiocarbamato)halogeno-iron(III)[30,35,36] and some tetraaza macrocyclic iron(III) com-

Table 4 Mössbauer parameters for $S = \frac{3}{2}$ iron(III) complexes

Complex	δ [a,b]	ΔE_Q [b,c]	$\frac{1}{2}\Gamma$ [b,d]	T/K	Donors	Ref.
1 [FeL(Cl)]	0.328(5)	2.543(9)	0.21(1) [e] 0.153(5) [f]	293	N_2S_2Cl	This work
	0.452(2)	2.824(7)	0.212(2) [e] 0.158(1) [f]	80	N_2S_2Cl	This work
	0.459(3)	2.806(5)	0.195(5) [e] 0.153(3) [f]	4.5	N_2S_2Cl	This work
$[Fe\{S_2CN(CH_3)_2\}_2Cl]$		2.66 [g]		1.2	S_4Cl	30
$[Fe\{S_2CN(C_2H_5)_2\}_2Cl]$	0.492(8)	2.70(1)		77	S_4Cl	29
		2.68(4) [g]		1.2	S_4Cl	30
$[Fe\{S_2CN(i\text{-}C_3H_7)_2\}_2Cl]$		2.68(3) [g]		1.2	S_4Cl	30
$[Fe\{S_2CN(C_2H_5)_2\}_2Br]$	0.492(8)	2.85(1)		77	S_4Br	29
		2.88(4) [g]		1.2	S_4Br	30
$[Fe\{S_2CN(C_2H_5)_2\}_2I]$	0.509(8)	2.89(1)		77	S_4I	29
$[Fe\{S_2CN(C_2H_5)_2\}_2(SCN)]$	0.509(8)	2.65(1)		77	S_5	29
$[Fe(Ph_2[15]aneN_4)(SPh)]$	0.13	2.55		77	N_4S	28
$[Fe(Ph_2[16]aneN_4)(SPh)]$	0.26	1.93		300	N_4S	28
		2.28		77	N_4S	28
$[FeL'(Cl)]^{2-}$	0.14	3.68		298	N_4Cl	31(*a*)
	0.25(3)	3.60(5)	0.17	4.2	N_4Cl	31(*a*)
$[FeL''(OH_2)]^-$	0.14	4.29		298	N_4O	31(*b*)
	0.14(2)	4.19(4)		4.2	N_4O	31(*b*)

[a] Isomer shift (mm s^{-1}). [b] Statistical standard deviations are given in parentheses. [c] Quadrupole splitting (mm s^{-1}). [d] Half-width. [e] Half-width of the low-energy line. [f] Half-width of the high-energy line. [g] No isomer shift data are available in ref 30; the quadrupole coupling constant $1/2e^2qQ$ was obtained from the best fit of the corresponding Zeeman spectrum.

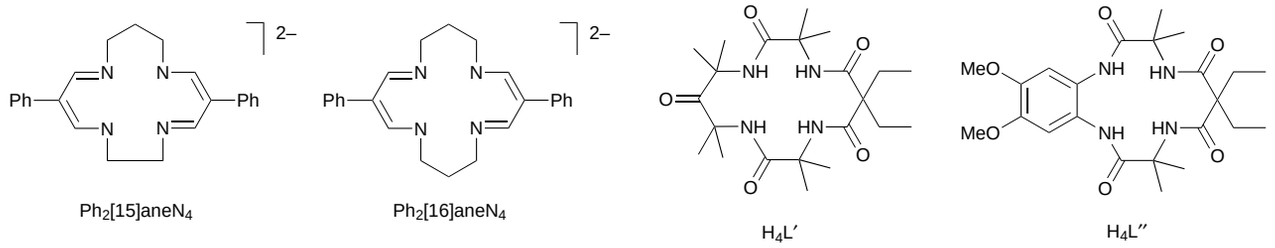

plexes,[28,31] iron(III) compounds are either low or high spin. Moreover, all pure intermediate-spin non-heme iron(III) complexes described so far have either a N_4X (with X = Cl, S or OH_2) or a S_4X (with X = Cl, I, Br, SCN, *etc.*) co-ordination sphere. Thus **1** is the first example of $S = \frac{3}{2}$ iron(III) complexes with a mixed nitrogen–sulfur donor set, N_2S_2Cl. Evidence for a pure intermediate-spin state arises primarily from magnetic susceptibility and Mössbauer data. The magnetic moment is constant and equal to 3.8 μ_B over the 10–300 K range which is very close to the 3.87 μ_B spin-only value expected for $S = \frac{3}{2}$. The isomer shift and quadrupole splitting values for complex **1** and their temperature dependence are similar to those observed for well characterized $S = \frac{3}{2}$ iron(III) spin systems (Table 4). Its powder and CH_2Cl_2 frozen-solution EPR spectra exhibit a broad main resonance located near to $g = 3.7$, reminiscent of the patterns observed for the $S = \frac{3}{2}$ bis(dithiocarbamato)-iron(III) complexes and more particularly the thiocyanato derivative.[35] The EPR spectra of $S = \frac{3}{2}$ iron(III) complexes experiencing a rhombically distorted cubic ligand field are usually characterized by three resonances with effective g values close to 2 for g_z and 4 for g_x and g_y, the separation of which is dependent upon the $\lambda = E/D$ rhombicity factor. However Chapps *et al.*[35] have shown that the broad EPR pattern of $[Fe\{S_2CN(C_2H_5)_2\}_2(SCN)]$ can be interpreted by a $\lambda = E/D$ rhombicity factor of 0.116 and linewidths of *ca.* 600 Oe. The molecular structure of complex **1** clearly indicates a significant rhombic distortion from the axial symmetry around the iron. It seems thus reasonable to suggest that the broad main resonance located at $g = 3.7$ arises from a combination of E/D ratio and linewidths close to those evaluated by Chapps *et al.* for $[Fe\{S_2CN(C_2H_5)_2\}_2(SCN)]$. Finally the presence of a weak resonance close to $g = 2$ and a broad unsymmetrical resonance with two maxima close to $g = 4.2$ and 3.4 in the powder spectra of complex **1** at 100 and 293 K further supports this interpretation. Several factors including exchange broadening (or narrowing) and spin–spin relaxation may contribute to the EPR linewidths; however, the prevailing factor is usually the latter. In the case of **1**, exchange broadening may be excluded on the basis of structural parameters and the temperature dependence of the EPR spectra, although small, seems to indicate that spin–spin relaxation is mainly responsible for the observed linewidths.

Similarly to all other $S = \frac{3}{2}$ iron(III) complexes, **1** exhibits a distorted square-pyramidal structure with a particularly long axial bond. As a result of this long Fe–Cl axial bond, the chloride ligand can easily be substituted by HO^- upon addition of tetrabutylammonium hydroxide. However the hydroxo complex could be only observed at the trace level by EPR spectroscopy (data not shown), the final complex **2** being the μ-oxo derivative.

Acknowledgements

This work was supported by a grant from Ministère de la Recherche et de la Technologie and Rhône-Poulenc (Programme Bioavenir) and a fellowship to Marie-Aude Kopf from Rhône-Poulenc. We thank Professor I. Morgenstern and Dr. A. Bousseksou for helpful discussions on the EPR and Mössbauer results.

References

1 P. J. Marini, K. S. Murray and B. O. West, *J. Chem. Soc.*, *Chem. Commun.*, 1981, 726.
2 G. D. Fallon, P. J. Nichols and B. O. West, *J. Chem. Soc.*, *Dalton Trans.*, 1986, 2271.
3 G. D. Fallon and B. M. Gatehouse, *J. Chem. Soc.*, *Dalton Trans.*, 1975, 1344.

4 P. J. Marini, K. S. Murray and B. O. West, *J. Chem. Soc.*, *Dalton Trans.*, 1983, 143.
5 R. H. Holm, in *Adv. Inorg. Chem.*, 1992, **38**, 1.
6 D. Coucouvanis, D. Swenson, N. C. Baenziger, C. Murphy, D. G. Holah, N. Sfarnas, A. Simopoulos and A. Kostikas, *J. Am. Chem. Soc.*, 1981, **103**, 3350.
7 R. Shukla and P. K. Bharadwaj, *Polyhedron*, 1993, **16**, 1983.
8 S. C. Shoner, D. Barnhart and J. A. Kovacs, *Inorg. Chem.*, 1995, **34**, 4517.
9 T. Beissel, K. S. Bürger, G. Voigt, K. Wieghardt, C. Butzlaff and A. X. Trautwein, *Inorg. Chem.*, 1993, **32**, 124.
10 N. Govindaswamy, D. A. J. Quarless and S. A. Koch, *J. Am. Chem. Soc.*, 1995, **117**, 8468.
11 Y. Sugiura, J. Kuwahara, T. Nagasawa and H. Yamada, *J. Am. Chem. Soc.*, 1987, **109**, 5848; M. A. Kopf, D. Bonnet, I. Artaud, D. Petre and D. Mansuy, *Eur. J. Biochem.*, 1996, **240**, 239.
12 M. J. Nelson, H. Y. Jin, I. M. Turner, G. Grove, R. C. Scarrow, B. A. Brennan and L. Que, *J. Am. Chem. Soc.*, 1991, **113**, 7072.
13 B. A. Brennan, J. G. Cummings, D. B. Chase, I. M. Jr. Turner and M. J. Nelson, *Biochemistry*, 1996, **35**, 10 068.
14 R. C. Scarrow, B. A. Brennan, J. G. Cummings, H. Jin, D. J. Duong, J. T. Kindt and M. J. Nelson, *Biochemistry*, 1996, **35**, 10 078.
15 H. V. Jin, I. M. Turner, M. J. Nelson, R. J. Gurbiel, P. E. Doan and B. M. Hoffman, *J. Am. Chem. Soc.*, 1993, **115**, 5290.
16 P. E. Doan, M. J. Nelson, H. Jin and B. M. Hoffman, *J. Am. Chem. Soc.*, 1996, **118**, 7014.
17 W. Huang, J. Jia, J. Cummings, M. Nelson, G. Schneider and Y. Lindquist, *Structure*, 1997, **5**, 691.
18 F. Varret, *Proceedings of the International Conference on Mössbauer Effect Applications*, *Jaipur*, *1981*, Indian National Science Academy, New Delhi, 1982.
19 D. J. Watkin, J. R. Carruthers and P. W. Betteridge, in *Crystals, An Advanced Crystallographic Program System*, Chemical Crystallography Laboratory, University of Oxford, 1988.
20 *International Tables for X-Ray Crystallography*, Kynoch Press, Birmingham, 1974, vol. 4.
21 G. M. Sheldrick, SHELXS 86, Program for Crystal Structure Solution, University of Göttingen, 1986.
22 M. M. Klenk, C. M. Suter and S. Archer, *J. Am. Chem. Soc.*, 1948, **70**, 3846.
23 J. M. Berg and R. H. Holm, *J. Am. Chem. Soc.*, 1985, **107**, 917.
24 R. Adams and S. Miyano, *J. Am. Chem. Soc.*, 1954, **76**, 3168.
25 P. Bamfield and P. M. Quan, *Synthesis*, 1978, 537.
26 J. C. Rodriguez-Ubis, B. Alpha, D. Plancherel and J. M. Lehn, *Helv. Chim. Acta*, 1984, **67**, 2264.
27 N. N. Greenwood and T. C. Gibbs, *Mössbauer Spectroscopy*, Chapman and Hall, New York, 1971.
28 S. Koch, R. H. Holm and R. B. Frankel, *J. Am. Chem. Soc.*, 1975, **97**, 6714.
29 D. Mansuy, I. Morgenstern-Badarau, M. Lange and P. Gans, *Inorg. Chem.*, 1982, **21**, 1427.
30 H. H. Wickman and A. M. Trozzolo, *Inorg. Chem.*, 1968, **7**, 63.
31 (*a*) K. L. Kostka, B. G. Fox, M. P. Hendrich, T. J. Collins, C. E. F. Rickard, L. J. Wright and E. Münck, *J. Am. Chem. Soc.*, 1993, **115**, 6746; (*b*) M. J. Bartos, C. Kidwell, K. E. Kaufmann, S. W. Gordon-Wylie, T. J. Collins, G. C. Clark, E. Münck and S. T. Weintraub, *Angew. Chem.*, *Int. Ed. Engl.*, 1995, **34**, 1216.
32 J. N. Mukherjee, A. J. Abrahamson, G. S. Patterson, T. D. P. Stack and R. H. Holm, *Inorg. Chem.*, 1988, **27**, 2137.
33 G. P. Gupta, G. Lang, W. R. Scheidt, D. K. Geiger and C. A. Reed, *J. Chem. Phys.*, 1986, **85**, 5212.
34 G. P. Gupta, G. Lang, C. A. Reed, K. Shelly and W. R. Schedit, *J. Chem. Phys.*, 1987, **86**, 5288.
35 G. E. Chapps, S. W. McCann, H. H. Wickman and R. C. Sherwood, *J. Chem. Phys.*, 1974, **60**, 990.
36 R. L. Martin and A. H. White, *Inorg. Chem.*, 1967, **6**, 712.

Received 15*th September* 1997; *Paper* 7/06664C